IEEE Photonics Journal
An IEEE Photonics Society Publication

Open Access

The Focusing Property of Immersed Plasmonic Nanolenses Under Radially Polarized Illumination

Volume 5, Number 2, April 2013

Er-Wei Wang
Ling-Li Li
Wei-Xing Yu
Tai-Sheng Wang
Jin-Song Gao
Yong-Qi Fu
Yu-Ling Liu

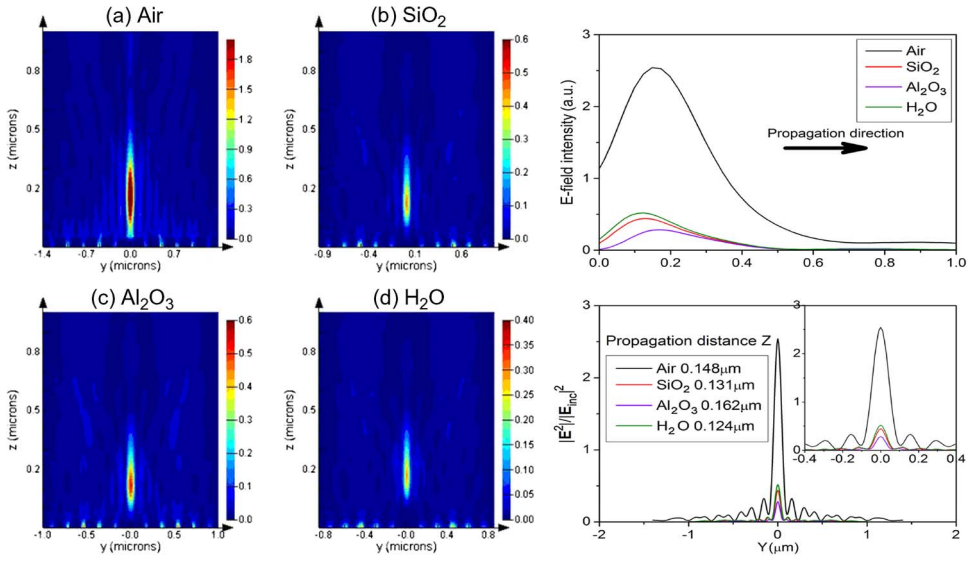

DOI: 10.1109/JPHOT.2013.2246558
1943-0655/$31.00 ©2013 IEEE

IEEE photonics SOCIETY

IEEE

The Focusing Property of Immersed Plasmonic Nanolenses Under Radially Polarized Illumination

Er-Wei Wang,[1,2] Ling-Li Li,[1,2] Wei-Xing Yu,[1] Tai-Sheng Wang,[1] Jin-Song Gao,[1] Yong-Qi Fu,[3] and Yu-Ling Liu[4]

[1]State Key Laboratory of Applied Optics, Changchun Institute of Optics, Fine Mechanics and Physics, Chinese Academy of Sciences, Changchun 130033, China
[2]University of Chinese Academy of Sciences, Beijing 10039, China
[3]School of Physical Electronics, University of Electronic Science and Technology of China, Chengdu 610054, China
[4]College of Science, Zhejiang University of Technology, Hangzhou 310023, China

DOI: 10.1109/JPHOT.2013.2246558
1943-0655/$31.00 ©2013 IEEE

Manuscript received December 22, 2012; revised February 2, 2013; accepted February 6, 2013. Date of current version February 26, 2013. This work was supported in part by the Ministry of Science and Technology of China under Grant 2010DFR10660 and Grant 2011DFA50590 and in part by Zhejiang Provincial Natural Science Foundation of China under Grant Y1111024. Corresponding author: W.-X. Yu (e-mail: yuwx@ciomp.ac.cn).

Abstract: The focusing property of immersed plasmonic nanolenses was theoretically studied by a rigorous electromagnetic numerical analysis method. The immersed plasmonic nanolens consists of a through central hole surrounded by a set of concentric slits with a period of plasmonic wavelength. The computational results show that the focusing property of immersed plasmonic nanolenses is, in general, similar to that of traditional immersion lenses. Normally, for the given incident wavelength, the higher the refractive index of the immersed medium, the smaller the focusing spot. For different wavelengths, the focusing property of immersed plasmonic nanolenses shows the similar focusing property, in comparison with traditional lenses, as well. A focal length of around half of the incident wavelength and the smallest focusing spot of less than a quarter of the incident wavelength have been achieved. The physical explanation of the different focusing behavior of immersed nanolenses is also given. The reported immersed plasmonic nanolens with a quasi-far-field focal length, as well as a superfocusing spot, can find applications in areas including nanolithography, data storage, super-resolution imaging, and so on.

Index Terms: Plasmonic nanolenses, subwavelength structures, nanostructures.

1. Introduction

In recent years, plasmonic nanostructures have gained lots of interests from researchers with regard to their great potential applications in super-resolution imaging, data storage, near-field microscopy, sensing, and nanolithography [1]–[7]. As a result, some new effects in plasmonics have been discovered and benefited a variety of research fields [8]–[14]. Recently, the Talbot effect from plasmonic nanolenses has been studied under the illumination of radially polarized light condition, and it is shown that the formed focusing spot has surpassed the diffraction limit [10]. In order to obtain focal spots with dimensions far less than the diffraction limited, the focusing property of the plasmonic nanolenses immersed in different media illuminated by a radially polarized light with different wavelengths was computationally studied in this paper. The results show that immersed

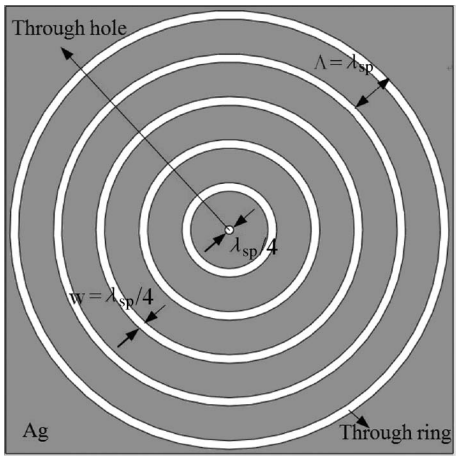

Fig. 1. Schematic diagram of the immersed plasmonic nanolens.

plasmonic nanolenses have the superior focusing property that follows the similar rule in comparison with traditional lenses.

2. Structure Description and Simulation Setup

As shown in Fig. 1, we considered the Ag-, Au-, and Al-based nanolenses with thickness of $d = 100$ nm, an on-axis hole of $\lambda_{sp}/4$ in diameter surrounded by a set of five periodic concentric rings with a lattice constant of $\Lambda = \lambda_{sp}$, and ring width $w = \lambda_{sp}/4$. Here, λ_{sp} stands for the surface plasmonic wavelength. The concentric ring slits are etched through into the metal film, and the slits are filled with the immersion medium. The reason why we choose the ring width as $\lambda_{sp}/4$ is because the sidelobes of the focusing spot of the plasmonic nanolens can be effectively suppressed, whereas the total transmitted E-field intensity can still be maintained strong enough [1]. Different from previous study, the designed plasmonic nanolens is immersed in the same medium, which means that, in the model, the media before and after the nanolens are identical. The immersion media we considered here are air, SiO_2, Al_2O_3, and H_2O.

The light source being used here is a Z-normal radially polarized Gaussian beam, and the beamwidth in the X-direction is equal to that in the Y-direction, which was designed to be $10\lambda_{sp}$. As for nanolithography, UV light is normally used. Therefore, in this article, UV light sources with wavelengths of 248, 365, and 442 nm were chosen as the incident light sources. The axis of symmetry of the slits coincides with the optical axis of the incident radially polarized beam. Intensity of the incident light propagating along the positive Z-direction was assumed to be 1 in the calculation. A rigorous finite-difference and time-domain (FDTD) algorithm was employed in the computational numerical simulation. In our 3-D numerical simulations, simulation time was set as 150 fs and mesh sizes of Δx, Δy, and Δz were generated by the software (FDTD solutions, Lumerical) to make sure the grid number in the nanostructure is an integer. The perfectly matched layer boundary condition was applied at the simulation boundaries.

3. Results and Discussions

Fig. 2(a)–(d) shows the E-field distribution of Ag-based nanolenses in different media for $\lambda_{in} =$ 248 nm on a Y–Z plane at $X = 0$. Four different immersion media, i.e., air, SiO_2, Al_2O_3, and H_2O were used as the immersion materials, and their refractive indices for $\lambda_{in} = 248$ nm are 1.0003, 1.50841, 1.834, and 1.36288, respectively. As can be seen, there is only one focal region located at around half of the incident wavelength position after the exit plane $(Z = 0\ \mu m)$ of the Ag-film-based nanolens and the focal depth is rather long, i.e., $\sim\lambda_{in}$. The reason why focal spot falls into the quasi-far-field region can be explained in terms of the weak coupling of the propagating wave with the metallic slit cavity resonance mode [7], [15]. As the refractive indices of the immersed

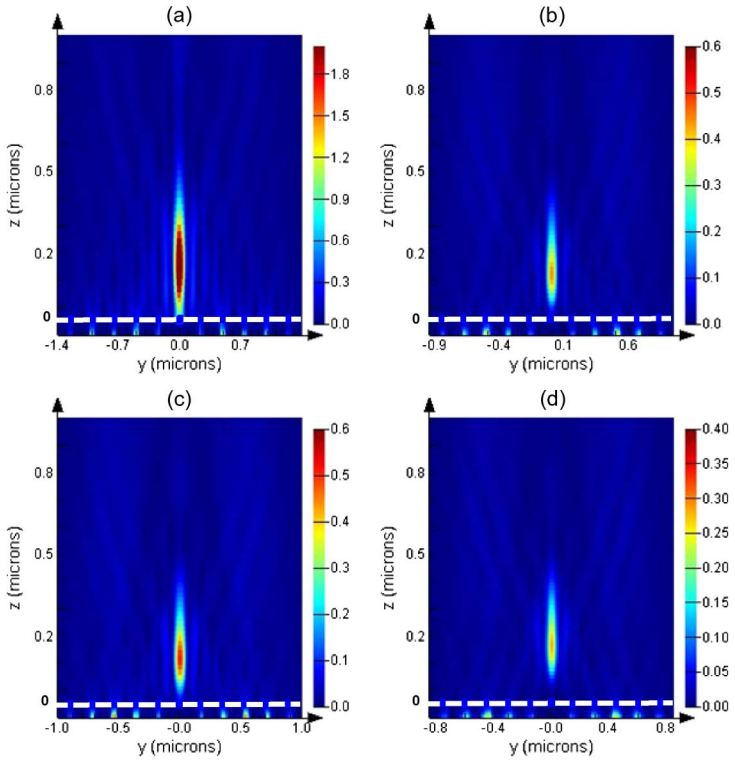

Fig. 2. Calculated E-field intensity distribution of the Ag-based nanolenses at Y–Z plane, $X = 0$, in different immersion media of (a) air, (b) SiO_2, (c) Al_2O_3, and (d) H_2O, respectively. The dashed white line in each subfigure indicates the exit plane of the plasmonic nanolens.

media here are all much greater than the plasmon resonance frequency, therefore the excited surface plasmon wave is quite weak so that the propagating wave is possible to go relatively farther. It should also be noted that the plasmonic nanolenses studied here are unlike those plasmonic nanolenses that have focal lengths equal to a few wavelengths in terms of the structure as well as the focusing mechanism [16]. On one side, those plasmonic nanolenses have no central hole and have corrugations on both sides of the metal film. On the other side, the focusing spots of those plasmonic nanolenses are formed by constructive interference of far-field radiation of surface plasmon polaritons (SPPs) generated on the back side of the lenses without contributions from other waves. However, in our case, there are central holes and through slits in plasmonic nanolenses, and the focal spots are formed with the contribution from both the propagating wave and the SPPs.

Fig. 3 shows the electric field distribution in the Z-direction at $X = Y = 0$. As can be seen clearly, there is only one peak transmission after the exit plane $(Z = 0\ \mu m)$ of the Ag-film-based nanolens. Specifically, the intensity of the focal point has the strongest intensity when the nanolens is immersed in air, and the calculated maximum intensity of 2.5 is attributed to the local enhanced extraordinary transmission contributed from strong coupling between SPP wave and propagating wave through the slits. However, the peak values of the focusing spots in other media are at the scale of < 0.5, which means stronger absorption or higher reflection of UV light in those immersed media exists. The size of the focusing spots follows the traditional case, i.e., the higher the refractive index of the immersed medium, the smaller the focusing spot. The smallest focusing spot appears in Al_2O_3, which is 60 nm, i.e., $< \lambda_{in}/4$. However, the anomalous phenomenon happens for the focusing distance, which does not follow the traditional case any more. For the traditional case, the higher the refractive index of the immersed medium, the shorter the focal length. For the plasmonic nanolenses studied here, the shortest focal distance is 120 nm, which appears in H_2O and corresponds to an $F^{\#}$ of 0.13 and a numerical aperture of 1.33. The longest focal distance is 160 nm, which appears in Al_2O_3 and corresponds to an $F^{\#}$ of 0.21 and a numerical aperture of

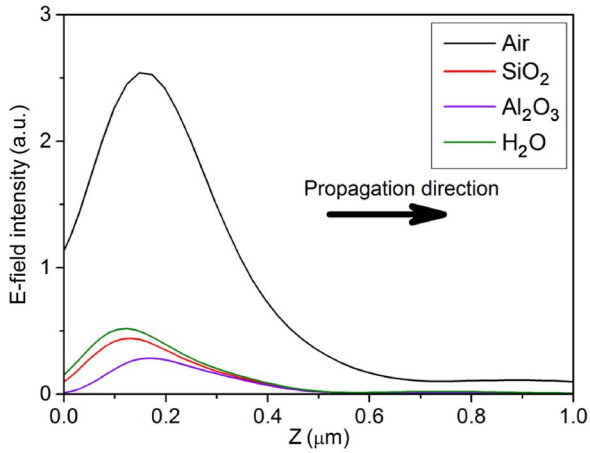

Fig. 3. Electric field transmission of the Ag-based nanolenses in four different immersion media (see the legend) at the incident wavelength $\lambda_{in} = 248$ nm in the Z-direction at $X = Y = 0$. The propagation direction is, from left to right, as shown in the figure. The exit plane is at $Z = 0$ μm.

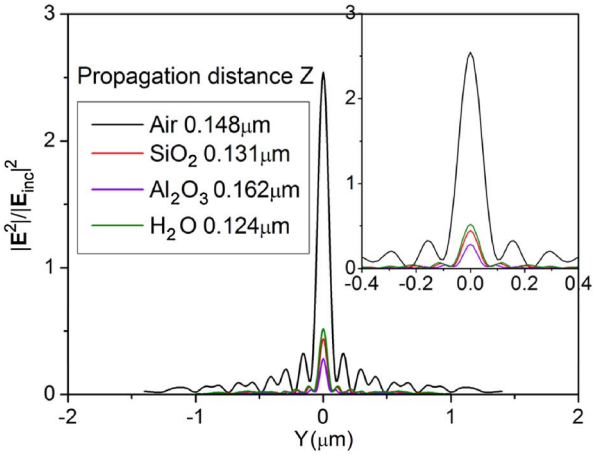

Fig. 4. Distributions of electric field intensity $|E|^2$ when the Ag-based nanolens is immersed in air, SiO_2, Al_2O_3, and H_2O at $\lambda_{in} = 248$ nm in Y–Z plane at $X = 0$ at the corresponding focal positions of $Z = 0.148$, 0.131, 0.162, and 0.124 μm, respectively.

1.834. This means that the immersed medium with the highest refractive index does have the highest numerical aperture and the corresponding smallest focusing spot. This also follows the traditional lens situation. However, the anomalous focal length property can be explained in terms of the different plasmonic wavelengths in different immersed media and the different apertures of the plasmonic nanolens. As for H_2O, $\lambda_{sp} = 184$ nm and the corresponding diameter of the plasmonic nanolens is $10\lambda_{sp} = 1840$ nm, whereas for Al_2O_3, $\lambda_{sp} = 146$ nm and the corresponding diameter of the plasmonic nanolens is $10\lambda_{sp} = 1460$ nm. Therefore, although the focal length of the nanolens in H_2O is only 120 nm, which is much shorter than that in Al_2O_3, but considering the larger diameter of the nanolens in H_2O than in Al_2O_3, the numerical aperture of the nanolens in H_2O becomes smaller than that in Al_2O_3.

To further compare their focusing properties, the intensity profiles of the focal spots at the corresponding focal positions of $Z = 0.148$, 0.124, 0.131, and 0.162 μm for air, H_2O, SiO_2, and Al_2O_3, respectively, are presented in Fig. 4. The diameters at the site of full-width at half-maximum (FWHM) of the focusing spot are 98, 72, 68, and 60 nm for air, H_2O, SiO_2, and Al_2O_3 immersion, respectively. After analyzing the properties of the intensity profiles, it can be seen that the minimum

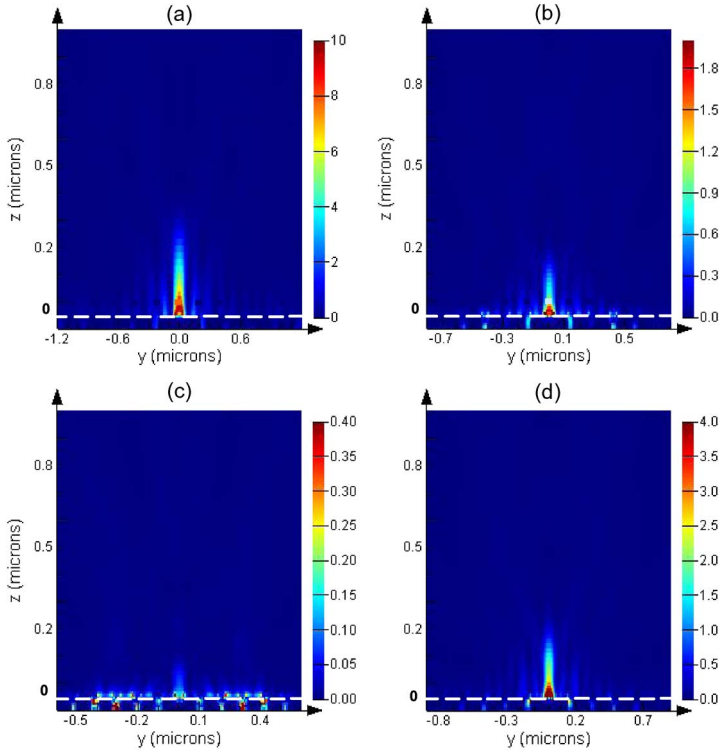

Fig. 5. Calculated E-field intensity distribution of the Al-based nanolens in Y–Z plane at X = 0 for 248-nm incident wavelength in different immersion media of (a) air, (b) SiO_2, (c) Al_2O_3, and (d) H_2O, respectively. White dashed line indicates the exit plane of the nanolens.

round beam spot (FWHM = 60 nm) is obtained when the nanolens is immersed in Al_2O_3, which is less than a quarter of λ_{in} (248 nm) and suggesting the resolving power has surpassed the diffraction limit. The maximum focusing spot (FWHM = 98 nm) is obtained when the nanolens is immersed in air. This trend seems follow the rule of the traditional lens very well. For traditional lenses, the higher the refractive index of the immersed medium, the smaller the focusing spot. Here, for plasmonic nanolens, it is the same. However, unlike the traditional lenses, the smallest focusing spot does not correspond to the shortest focal distance. This can be explained from the aspect of the plasmonic wavelength. As we know, for different immersed media, the plasmonic wavelength is different. Specifically for the immersed nanolenses studied here, the plasmonic wavelength is $\lambda_{sp} = 249$, 184, 170, and 146 nm for air, H_2O, SiO_2, and Al_2O_3, respectively. Hence, the corresponding diameter of the plasmonic nanolenses is $10\lambda_{sp} = 2.49$, 1.84, 1.70, and 1.46 μm for air, H_2O, SiO_2, and Al_2O_3, respectively. Therefore, the corresponding F number is 0.06, 0.065, 0.076, and 0.11 for air, H_2O, SiO_2, and Al_2O_3, respectively, and the corresponding numerical aperture is 0.993, 1.367, 1.491, and 1.791 for air, H_2O, SiO_2, and Al_2O_3, respectively. As can be seen, in this case, the higher the refractive index of the immersed medium, the smaller the focal spot. This totally follows the rule of traditional lenses.

By using the same method, the Au- and Al-based plasmonic nanolenses immersed in different media for $\lambda_{in} = 248$ nm were analyzed. Fig. 5 shows the E-field distribution of Al-based nanolenses in different media for $\lambda_{in} = 248$ nm on a Y–Z plane at X = 0. As clearly shown in Fig. 5, there is no focusing spot in the quasi-far-field area for the Al-based plasmonic nanolens, which means the focusing surface plasmonic wave is strictly confined on the surface of the nanolens and cannot propagate away like the case shown in Fig. 2. The reason why Al-based nanolenses behave differently in comparison with Ag-based nanolenses can be attributed to the much stronger coupling of the propagating wave with the metallic slit cavity mode. In that the refractive indices of the immersed media are smaller or closer to the plasmon resonant wavelength, the surface plasmon

TABLE 1

Focal distance, FWHM of the focal spot, and $|E|^2$ Intensity of the immersed plasmonic nanolenses made in different materials for the different incident wavelengths in Y–Z plane

Nanolens material	Au											
Incident wavelength (nm)	248				365				442			
Immersion medium	Air	H_2O	SiO_2	Al_2O_3	Air	H_2O	SiO_2	Al_2O_3	Air	H_2O	SiO_2	Al_2O_3
Focal distance Z (μm)	99	120	82	108	180	160	120	120	260	200	150	120
FWHM of the focal spot (nm)	94	70	64	55	142	106	96	80	174	130	118	97
Intensity (a.u.)	2.68	0.8	0.5	0.18	5	2.97	1.8	0.95	4.95	2.5	1.77	1.01
Plasmonic wavelength (nm)	247	180	165	138	363.76	270.4	247.6	205.5	436.36	323.87	295.7	244
Numerical aperture	0.997	1.367	1.501	1.812	0.995	1.338	1.468	1.781	0.993	1.33	1.459	1.772

resonance in the slit cavity is quite stronger. As shown in Fig. 5, the strongest E-field intensity that is as high as tenfolds can be obtained. Compared with Ag-based plasmonic nanolenses where surface plasmon resonance is relative weaker, the transmitted E-field of Al-based nanolenses is apparently locally enhanced in the near field. Whereas for Au-based plasmonic nanolenses, the result is similar to the Ag-based plasmonic nanolens case; therefore, the E-field distribution is not shown here. Table 1 shows the calculation results of Au-based plasmonic nanolenses in various immersed media for a 248-nm incident wavelength. The results show that the smallest focusing spot of 55 nm can be obtained in Al_2O_3, which indicates that a smaller focusing spot can be obtained in Al_2O_3 for the Au-based plasmonic nanolens in comparison with the Ag-based plasmonic nanolens.

To further study the focusing property of immersed plasmonic nanolenses, the conditions for different incident wavelengths, 365 and 442 nm, were also analyzed. The calculation results indicate that, for these two wavelengths, both the Ag- and Al-based plasmonic nanolenses cannot obtain the quasi-far-field focusing spots, and the transmitted light field is strictly confined on the interface of the metal/dielectric like that of the Al-based nanolens at the 248-nm incident wavelength. Again, the different behavior of plasmonic nanolenses at these two wavelengths can be explained in terms of the coupling degree of the propagating wave and the metallic slit cavity mode. Therefore, only the summary of the focusing property of the Au-based plasmonic nanolens for wavelengths of 365 and 442 nm is listed in Table 1.

For cases of $\lambda_{in} = 365$ and 442 nm, the focusing property of the immersed nanolens is similar to that of the case $\lambda_{in} = 248$ nm. In general, the focusing spot of the immersed nanolens follows the same rule with the traditional lens. That is, the higher the refractive index of the medium is, the smaller the focal spot is. The minimum focal spot obtained for $\lambda_{in} = 365$ and 442 nm is 80 and 97 nm, respectively. Again, the focusing spots are less than a quarter of incident wavelength, and this means the diffraction limit has been broken. In comparison with $\lambda_{in} = 248$ nm case, the E-field intensity of the focusing spot for both cases is nearly unit, which means a strong local enhanced field transmission has been achieved.

4. Summary

In summary, the immersed plasmonic nanolens shows the similar focusing property in comparison with the traditional lens. Normally, for the same incident wavelength, the higher the refractive index of the immersed medium, the smaller the focusing spot. For different wavelengths, the focusing

property of plasmonic nanolens shows the similar focusing property in comparison with the traditional lens as well. Moreover, it is found that, for longer wavelengths, the local field enhancing phenomenon becomes pronouncing. However, it should be noted that the conclusion reported in this article only applies when the diameter of the plasmonic nanolens changes accordingly when the immersion medium and the incident wavelength change. This is because the plasmonic wavelength will be changed when those related physical parameters are changed. Finally, it is found that the best performing immersed plasmonic nanolens has an FWHM of as small as $\lambda_{in}/4$ for the focal spot falling in the quasi-far field and an elongated focal depth of $\sim\lambda_{in}$, which will make the plasmonic nanolens very promising for nanolithography in that the relatively long working distance and focal depth will make the process easier to control. Of course, it can also find potential applications in data storage, super-resolution imaging, and others.

References

[1] W. X. Yu, Y. Q. Fu, L. L. Li, H. X. Zhang, H. Liu, Z. W. Lu, and Q. Sun, "Computational study of influence of structuring of plasmonic nanolens on superfocusing," *Plasmonics*, vol. 6, no. 1, pp. 35–42, Mar. 2011.

[2] F. I. Baida and A. Belkhir, "Superfocusing and light confinement by surface plasmon excitation through radially polarized beam," *Plasmonics*, vol. 4, no. 1, pp. 51–59, Mar. 2009.

[3] W. Chen, D. C. Abeysinghe, R. L. Nelson, and Q. Zhan, "Plasmonic lens made of multiple concentric metallic rings under radially polarized illumination," *Nano. Lett.*, vol. 9, no. 12, pp. 4320–4325, Dec. 2009.

[4] Y. Fu, W. Zhou, and L. Lim, "Plasmonic microzone plate: Superfocusing at visible regime," *Appl. Phys. Lett.*, vol. 91, no. 6, pp. 061124-1–061124-3, Aug. 2007.

[5] J. M. Steele, Z. Liu, Y. Wang, and X. Zhang, "Resonant and non-resonant generation and focusing of surface plasmons with circular gratings," *Opt. Exp.*, vol. 14, no. 12, pp. 5664–5670, Jun. 2006.

[6] F. J. García-Vidal, L. Martin-Moreno, H. J. Lezec, and T. W. Ebbesen, "Focusing light with a single subwavelength aperture flanked by surface corrugations," *Appl. Phys. Lett.*, vol. 83, no. 22, pp. 4500–4502, Dec. 2003.

[7] L. L. Li, Y. Q. Fu, H. S. Wu, L. G. Zheng, H. X. Zhang, Z. W. Lu, Q. Sun, and W. X. Yu, "The Talbot effect of plasmonic nanolenses," *Opt. Exp.*, vol. 19, no. 20, pp. 19 365–19 373, Sep. 2011.

[8] A. A. Maradudin and T. A. Leskova, "The Talbot effect for a surface plasmon polariton," *New J. Phys.*, vol. 11, no. 3, p. 033004, Mar. 2009.

[9] J. G. Sucerquia, D. C. A. Palacio, and H. J. Kreuzer, "High resolution Talbot self-imaging applied to structural characterization of self-assembled monolayers of microspheres," *Appl. Opt.*, vol. 47, no. 26, pp. 4723–4728, Sep. 2008.

[10] M. R. Dennis, N. I. Zheludev, and F. J. García de Abajo, "The plasmon Talbot effect," *Opt. Exp.*, vol. 15, no. 15, pp. 9692–9700, Jul. 2007.

[11] E. E. Moon, L. Chen, P. N. Everett, M. K. Mondol, and H. I. Smith, "Nanometer gap measurement and verification via chirped-Talbot effect," *J. Vac. Sci. Technol. B*, vol. 22, no. 6, pp. 3378–3381, Nov. 2004.

[12] I. I. Smolyaninov and C. C. Davis, "Apparent superresolution in near-field optical imaging of periodic gratings," *Opt. Lett.*, vol. 23, no. 17, pp. 1346–1347, Sep. 1998.

[13] G. M. Lerman, A. Yanai, and U. Levy, "Demonstration of nanofocusing by the use of plasmonic lens illuminated with radially polarized light," *Nano. Lett.*, vol. 9, no. 5, pp. 2139–2143, May 2009.

[14] A. Yanai and U. Levy, "Plasmonic focusing with a coaxial structure illuminated by radially polarized light," *Opt. Exp.*, vol. 17, no. 2, pp. 924–932, Jan. 2009.

[15] A. P. Hibbins, M. J. Lockyear, and J. R. Sambles, "The resonant electromagnetic fields of an array of metallic slits acting as Fabry-Pérot cavities," *J. Appl. Phys.*, vol. 99, no. 12, pp. 124903-1–124903-5, Jun. 2006.

[16] P. Wróbel, J. Pniewski, T. J. Antosiewicz, and T. Szoplik, "Focusing radially polarized light by a concentrically corrugated silver film without a hole," *Phys. Rev. Lett.*, vol. 102, no. 18, pp. 183902-1–183902-4, May 2009.